Supporting Information

Sleiman et al. 10.1073/pnas.0912820107

SI Text

Experimental. ***Caution.*** *N*-nitroso nornicotine (NNN), 1-(*N*-methyl-*N*-nitrosamino)-1-(3-pyridinyl)-4-butanal) (NNA), and 4-(methylnitrosamino)-1-(3-pyridinyl)-1-butanone (NNK) are carcinogenic and mutagenic and should therefore be handled with extreme care at all times, inside a fume hood with ventilation. Appropriate personal protective equipment (nitrile gloves, lab coat, safety glasses) must also be used.

Results and Discussion. ***Nitrous acid (HONO) concentration profiles.*** In Fig. S2, HONO breakthrough curves are shown in the presence and absence of nicotine. For blank cellulose, the [HONO] profile resembled a weak acid titration curve, suggesting that uptake of HONO is governed by ionization equilibria in an aqueous surface layer. For nicotine-impregnated cellulose, HONO breakthrough was linear for more than 180 min, indicating the existence of a chemical sink related to direct interaction with nicotine.

The green dots depict the [HONO] consumed by nicotine, $\Delta[\mathrm{HONO}] = \sim 10$ ppb (20 ng cm^{-3}) corresponding to a reactive uptake rate $R_{\mathrm{HONO}} = 0.43$ ng min^{-1} cm^{-2} (5.5 μmol h^{-1} m^{-2}), defined as

$$R_{\mathrm{HONO}} = \frac{\Delta[\mathrm{HONO}] \cdot f}{S}, \qquad \textbf{[S1]}$$

where f is the air flow rate (in cm^3 min^{-1}) and S is the geometric exposed surface (in cm^2).

For $[\mathrm{HONO}] = 65$ ppb (2.6 μmol m^{-3}), a deposition mass-transfer coefficient of $k_{\mathrm{HONO}} = 2.1$ m h^{-1} can be estimated as follows:

$$k_{\mathrm{HONO}} = \frac{R_{\mathrm{HONO}}}{[\mathrm{HONO}]}. \qquad \textbf{[S2]}$$

By considering that k_{HONO} is the same order of magnitude as the boundary layer mass-transfer coefficient for the deposition of ozone (a reactive atmospheric specie) in buildings (1, 2), HONO uptake may be mass-transfer limited in the presence of surfaces loaded with nicotine. In those conditions, indoor HONO concentrations may be significantly reduced by this strong chemical sink.

Fitting of nicotine desorption curve. The nicotine desorption data shown in Fig. 1*B* were adjusted to a biexponential model (Eq. **S3**), to capture the two distinct regimes observed, corresponding to desorption (initial) and reaction with HONO:

$$\frac{[N]}{[N]_0} = A_1 \exp -\left(\frac{t}{\tau_1}\right) + A_2 \exp -\left(\frac{t}{\tau_2}\right), \qquad \textbf{[S3]}$$

in which $A_1 = 0.65$; $\tau_1 = 800$ min; $A_2 = 0.35$ and $\tau_2 = 15$ min.

Gas chromatography–ion trap–tandem mass spectrometry (GC-IT-MS/MS) chromatograms. In Fig. S3 we present GC-IT-MS/MS chromatograms for nine samples, to illustrate the sensitivity and selectivity of the method. Samples shown include the standard mixture of quinoline, nicotine, NNA and NNK in methanol, a blank extract of cellulose substrates exposed to HONO for 3 hours, an extract of cellulose loaded with nicotine and not exposed to HONO, an extract of cellulose loaded with nicotine and exposed to HONO (65 ppb) for 3 hours, labeled "Nic" in Fig. 1, an extract of cellulose exposed to secondhand smoke (SHS) in the chamber experiment, labeled "Sorbed SHS" in Fig. 1, an extract of a cellulose strip loaded with SHS and exposed to HONO (65 ppbv) for 3 hours, labeled "THS" in Fig. 1, an extract of cellulose placed for 3 days on the truck cabin of a smoker (labeled "Truck B" in Fig. 1), a blank extract of wipes used to collect samples of adsorbed organics in the truck cabin, and an extract of wipes used for sampling surfaces of truck cabin (labeled "Truck A" in Fig. 1).

Alternative reaction mechanism of nicotine with nitrous acid. Fig. S4 depicts an alternative pathway for tobacco-specific nitrosamine (TSNA) formation, consistent with a mechanism described by Hecht et al. in aqueous solution (3, 4). It involves initial nitrosation of nicotine by NO^+ leading to the formation of a nitrosoammonium cation, which undergoes elimination of a nitroxyl group to yield three isomeric imonium cations (5). Reaction of these cations with water, followed by HONO, generates the three TSNAs. This mechanism and that illustrated in Fig. 2*B* are both consistent with the formation of the observed TSNAs. Recent mechanistic studies of nicotine oxidation (6) support the mechanism shown in Fig. 2*B*, as the first step requires an oxidation-ring opening or demethylation prior to nitrosation. Nevertheless, further studies on reaction intermediates (not analyzed here) are needed to conclusively decide which of the two pathways is responsible for indoor TSNA formation.

Formation mechanisms and mass spectrum of 1-methyl-5-(3-pyridinyl) pyrazole. In Fig. S6, the intensity of the molecular ion m/z 159 is low because of intensive fragmentation on the MS (70 eV, 50 μA). Other analogous compounds such as β-nicotyrine, as well as the TSNAs, showed a similar fragmentation pattern. The base peaks were m/z 158 for the pyrazole and m/z 157 for β-nicotyrine, and they were separated chromatographically.

1. Morrison GC, Zhao P, Kasthuri L (2006) The spatial distribution of pollutant transport to and from indoor surfaces. *Atmos Environ* 40:3677–3685.
2. Cano-Ruiz JA, Kong D, Balas B, Nazaroff WW (1993) Removal of reactive gases at indoor surfaces: Combining mass transport and surface kinetics. *Atmos Environ* 27A:2039–2050.
3. Hecht SS, et al. (1978) Chemical studies on tobacco smoke. 52. Reaction of nicotine and sodium nitrite: Formation of nitrosamines and fragmentation of the pyrrolidine ring. *J Org Chem* 43:72–76.
4. Hecht SS, Chen C-HB, Hoffmann D (1979) Tobacco-specific nitrosamines: Occurrence, formation, carcinogenicity and metabolism. *Acc Chem Res* 12:92–98.
5. Smith PAS, Loeppky RN (1967) Nitrosative cleavage of tertiary amines. *J Am Chem Soc* 89:1147–1157.
6. Peterson LA, Castagnoli N (1988) Regio- and stereochemical studies on the α-carbon oxidation of (*S*)-nicotine by cytochrome P-450 model system. *J Med Chem* 31:637–640.

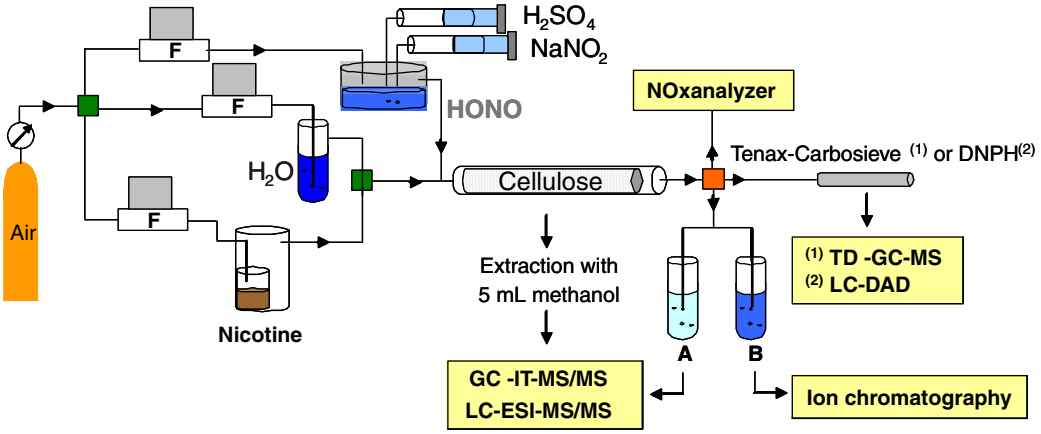

Fig. S1. Schematic of the experimental setup used for investigation of HONO reaction with nicotine sorbed on cellulose surfaces. (*A*) Methanol impinger; (*B*) NaOH (aq) impinger (pH = 10). All experiments were performed with a total air flow of 0.5 L min^{-1}, at relative humidity 45 ± 5% and $T = 23 \pm 2$ °C.

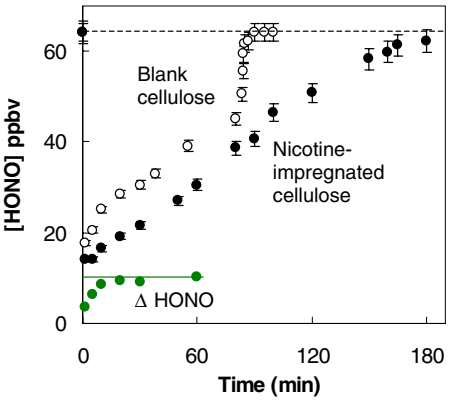

Fig. S2. HONO uptake by blank and nicotine-impregnated cellulose substrates. Constant upstream concentration was $[HONO]_0 = 65$ ppbv. Open and filled data points show downstream HONO breakthrough concentrations corresponding to two different conditions: uptake by a blank cellulose substrate and by nicotine-impregnated cellulose (9.1 μg cm^{-2}), respectively. Green dots correspond to the Δ[HONO] consumed by nicotine and determined by subtraction of the previous two data series.

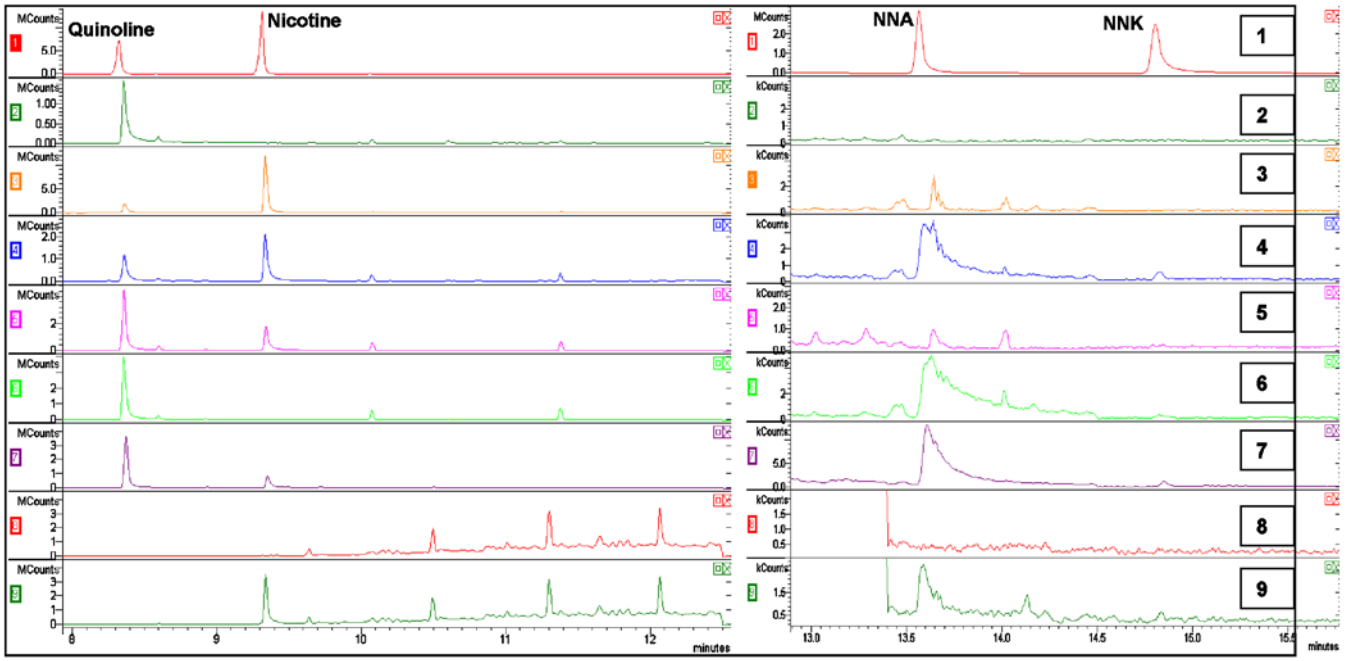

Fig. S3. GC-IT-MS/MS chromatograms of selected samples. (*1*) Standard mixture of quinoline, nicotine, NNA, and NNK in methanol. (*2*) Blank extract of cellulose paper exposed to HONO for 3 hours; (*3*) extract of cellulose paper loaded with nicotine and not exposed to HONO. Note that a chromatographic peak appears at 13.7 min near the retention time of NNA and likely originates from column bleeding. For quantification of NNA, only the specific ions 120 and 130 were used whereas interfering ions were subtracted. (*4*) Extract of cellulose strip loaded with nicotine and exposed to HONO (65 ppb) for 3 hours, labeled "Nic" in Fig. 1. (*5*) Extract of cellulose strip exposed to SHS in the chamber experiment, labeled "SHS" in Fig. 1. (*6*) Extract of cellulose strip loaded with SHS and exposed to HONO (65 ppbv) for 3 hours, labeled "THS" in Fig. 1. (*7*) Extract of cellulose paper placed for 3 days on the truck cabin of a smoker, labeled "Truck B" in Fig. 1. (*8*) Blank extract of wipes used to collect samples of adsorbed organics in the truck cabin. (*9*) Extract of wipes used for sampling surfaces of truck cabin, labeled "Truck A" in Fig. 1.

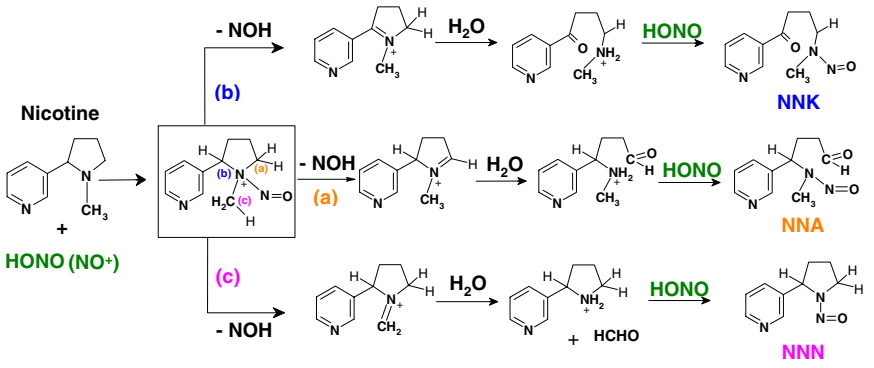

Fig. S4. Alternative mechanism for the formation of TSNAs. The first step involves the nitrosation of nicotine leading to the formation of nitroso-ammonium cation. The second step is initiated with an elimination of nitroxyl group to form an imonium cation, which is then hydrolyzed by sorbed water molecules. Finally the secondary amine formed can be subsequently nitrosated by HONO to form NNA, NNK, and NNN.

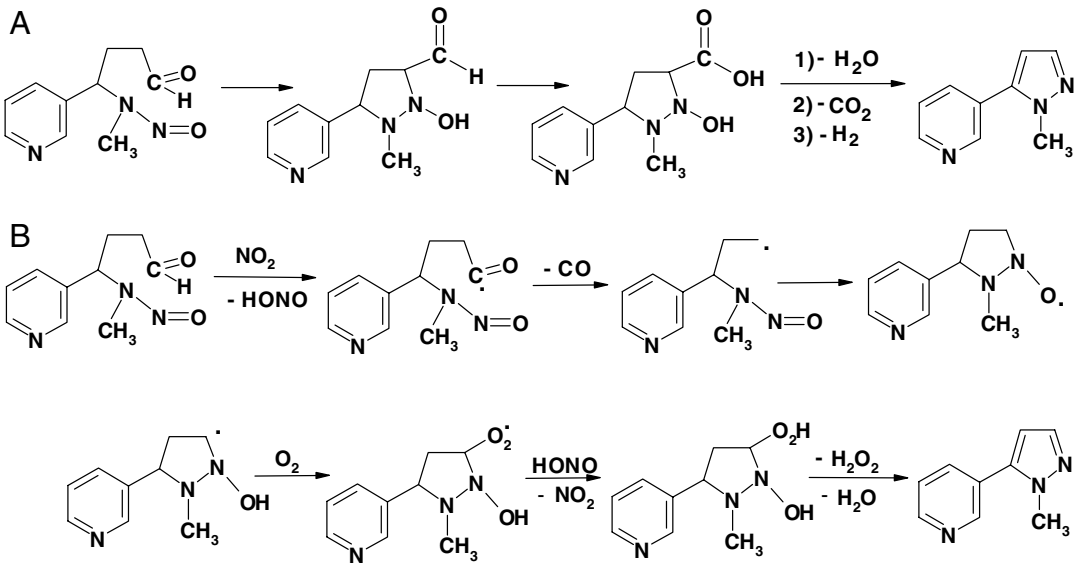

Fig. S5. Postulated mechanisms for the formation of 1-methyl-5-(3-pyridinyl) pyrazole from NNA. (*A*) According to refs. 3 and 4); (*B*) additional pathway proposed in this work.

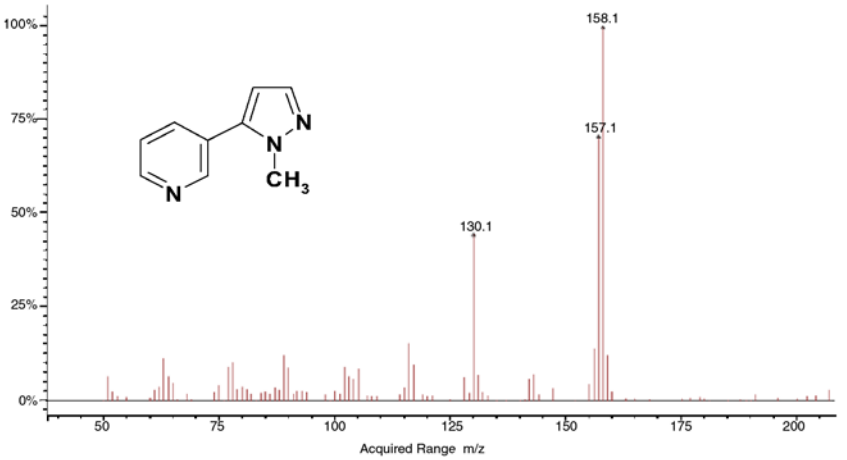

Fig. S6. Electron-impact (EI) mass spectrum of 1-methyl-5-(3-pyridinyl) pyrazole (secondary product number 7—Table 1)

Table S1. Experimental parameters for the chamber experiment with SHS

Parameter	
Chamber volume (m^3)	18
Cigarettes smoked	9
Temperature (°C)	24
Ventilated air-exchange rate (h^{-1})	1.0
Flow rate through filters (L min^{-1})	100
Filter sampling duration (min)	176
Volume of air samples with TCGF filter (m^3)	17.4
Net mass of particles on TCGF filter (mg)	17.8
SHS particle concentration (mg m^{-3})	1.02
Nicotine gas phase concentration (μg m^{-3})	60

Table S2. Experimental parameters for the field sampling experiment

Parameter	
Cigarettes smoked	34
Duration (days)	3
Exposed surface (cm^2)	262.5
Estimated HONO concentration (ppbv) (3)	10–30